SUPPORTING INFORMATION

Long-term prediction of climate change impacts on indoor particle pollution – case study of a residential building in Germany

Jiangyue Zhao[1], Tunga Salthammer[1,*], Alexandra Schieweck[1], Erik Uhde[1], Tareq Hussein[2,3]

1) Fraunhofer WKI, Department of Material Analysis and Indoor Chemistry, Riedenkamp 3, 38108 Braunschweig, Germany
2) University of Helsinki, Institute for Atmospheric and Earth System Research (INAR), PL 64, FI-00014, Helsinki, Finland
3) University of Jordan, School of Science, Department of Physics, Environmental and Atmospheric Research Laboratory (EARL), Amman, 11942 Jordan

*Author for Correspondence

Fraunhofer WKI

Department of Material Analysis and Indoor Chemistry

Riedenkamp 3

3808 Braunschweig, Germany

Phone: +49-531-2155-213

Email: tunga.salthammer@wki.fraunhofer.de

S1 Particle size-dependent penetration factors

Figure S1 shows the particle size-dependent penetration factors through various filters in mechanical ventilation. Note that the filters “F8”, “F7”, “F6”, “F5” and “G4” complied with the former EU standard DIN EN 779 for testing air filters,[1] which was replaced by the new international standard ISO 16890-1 in 2016.[2]

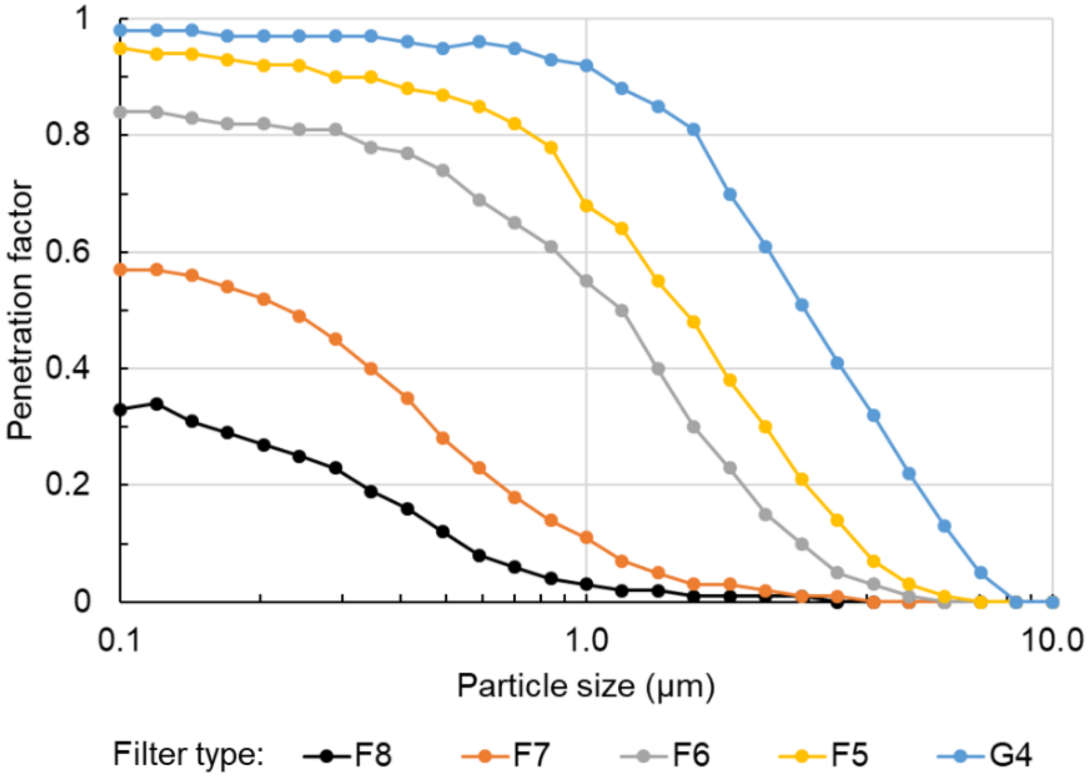

Figure S1. Particle size-dependent penetration factors through various filters in mechanical ventilation according to the filter efficiency data from Goodfellow and Tähti (2001).[3]

ISO 16890-1 defines four filter groups: Coarse, ePM_{10}, $ePM_{2.5}$ and ePM_1. A direct conversion between EN 779 and ISO 16890-1 is not possible. The two standards are based on different test conditions. There is a minimum level of ISO filtration that allows a comparison with EN 779 filters. Hemerka and Vybiral provided information for filter class conversion between EN 779 and ISO 16890-1.[4] In Table S1, the filter types from Figure S1 according to EN 779 are compared with the new filter types according to ISO 16890-1. An experimental verification of the ISO 16890-1 was carried out by Schuldt et al.[5]

Table S1. Comparison of filter types according to DIN EN 779[1] and ISO 16890-1.[2]

ISO 16890-1 (2016)	DIN EN 779 (2012)
ISO Coarse 60%	Corresponds to G4
	F5 (not defined in EN 779:2012)
	F6 (not defined in EN 779:2012)
ISO ePM_1 50%	Corresponds to F7
ISO $ePM_{2.5}$ 65%	Corresponds to F7
ISO ePM_1 70%	Corresponds to F8
ISO ePM_1 80%	Corresponds to F9 (data not shown in Figure S1)

S2 Particle model validation

In the test house, indoor and outdoor particle number size distribution (PNSD, 10 – 800 nm size range), $PM_{2.5}$ and PM_{10} data were collected during the (2016 - 2019) large measurement campaign in Germany – "Indoor and Outdoor Project" (UFOPLAN FKZ 3715 61 200, „Ultrafeine Partikel im Innenraum und in der Umgebungsluft: Zusammensetzung, Quellen und Minderungsmöglichkeiten").[6, 7] In addition, activity patterns (source type, frequency, and duration) of occupants in real-use conditions were also recorded. Detailed information on the measurement sites can be found in Zhao et al. (2020).[7] Briefly, two measurement systems were deployed to simultaneously measure indoor and outdoor particle parameters for each household. Each system includes a TROPOS-type mobile particle size spectrometer (MPSS) for the determination of PNSD and total particle number concentration (PNC) in the diameter range of 10-800 nm. Mass concentrations of PM_{10} and $PM_{2.5}$ were measured by an optical particle size spectrometer (OPSS Grimm, model 1.108). The instruments measure with a time resolution of 5 minutes. The selected test house is house L5 during the measurement campaign. The house was naturally ventilated. The data on air change rate and particle size-dependent penetration factors were taken from the results for this house published in our earlier work by Zhao et al.[8]

The model validation was applied for measurement on January 17, 2017 (see manuscript Section 2.4). The particle size-resolved emission rates of three activities on this day are listed in Table S2. The results of the measured and simulated PNSD, PNC, as well as particle mass concentrations of PM_1, $PM_{2.5}$ and PM_{10} are shown in Figure S2, Figure S3, and Figure S4, respectively.

Table S2. Particle size-resolved emission rates ×10^6 (# s^{-1}) for the three recorded indoor activities during the measurement on January 17, 2017 in the test house.

Activity	**Particle diameter D_p (nm)**											
	9	**12**	**15**	**20**	**26**	**39**	**64**	**105**	**173**	**286**	**472**	**778**
Toasting	13.9	116.7	249.2	382.2	466.4	697.4	503.2	107.6	12.7	2.3	0.2	0.0
Baking	59.7	124.6	202.9	221.3	240.7	441.0	434.6	180.7	73.4	16.2	3.5	0.9
Frying	2.6	34.8	55.7	66.6	70.6	108.3	80.4	27.9	10.7	3.3	0.9	0.4

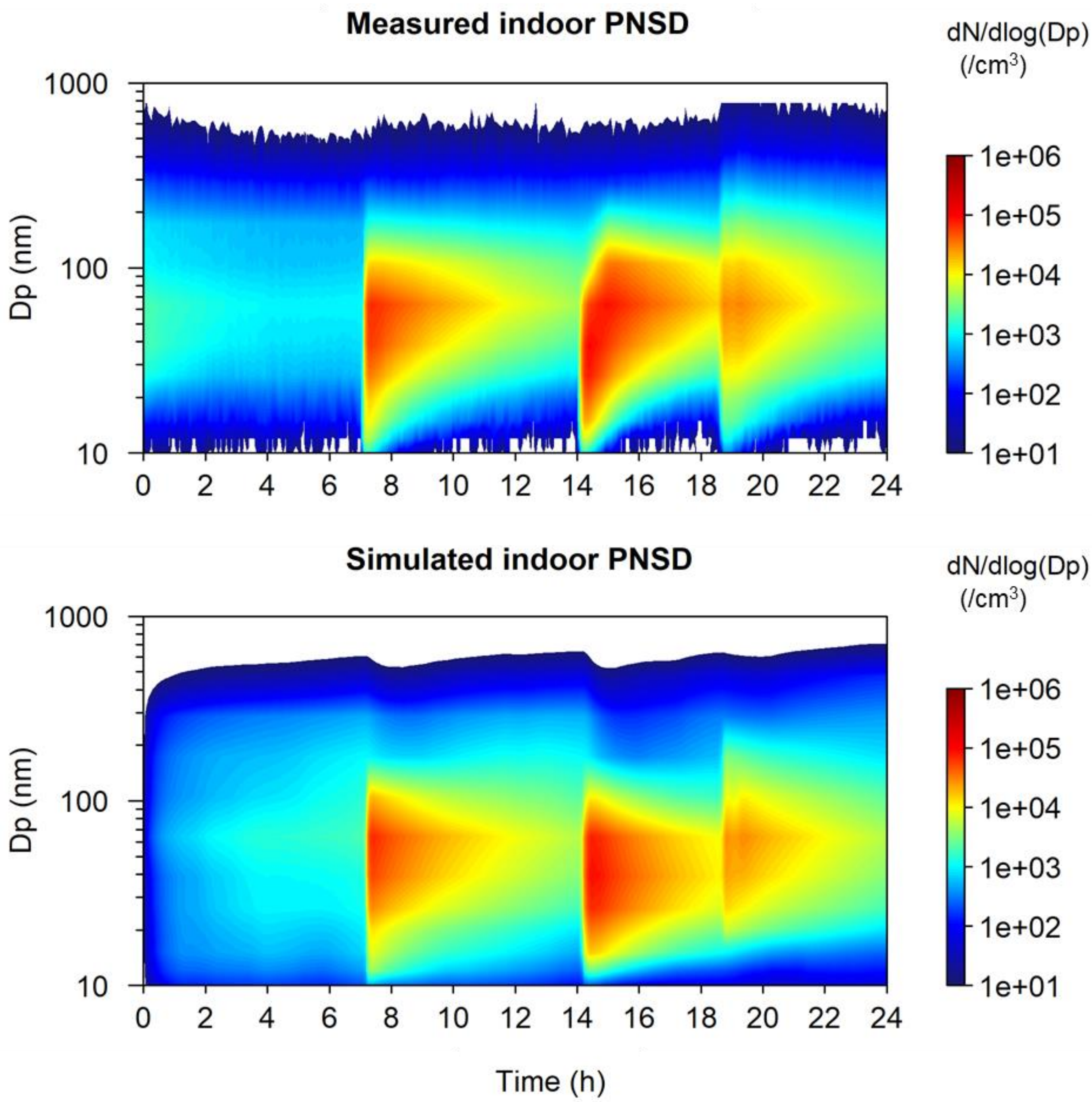

Figure S2. Comparison of measured and simulated indoor particle number size distribution.

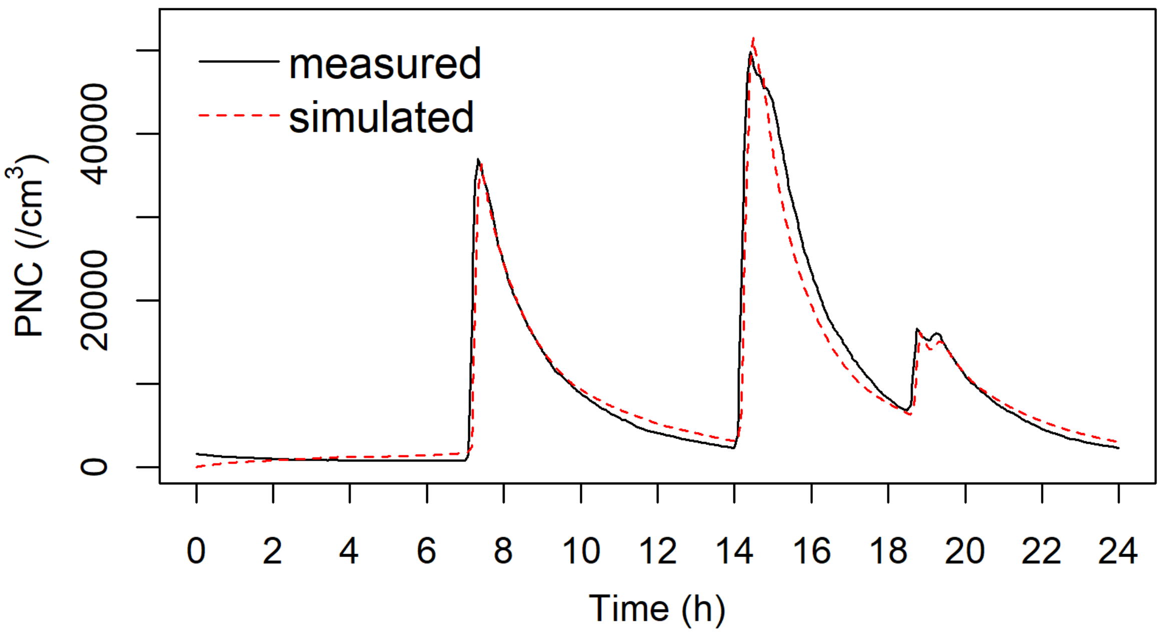

Figure S3. Comparison of indoor particle number concentrations calculated from PNSD data with measured and simulated values.

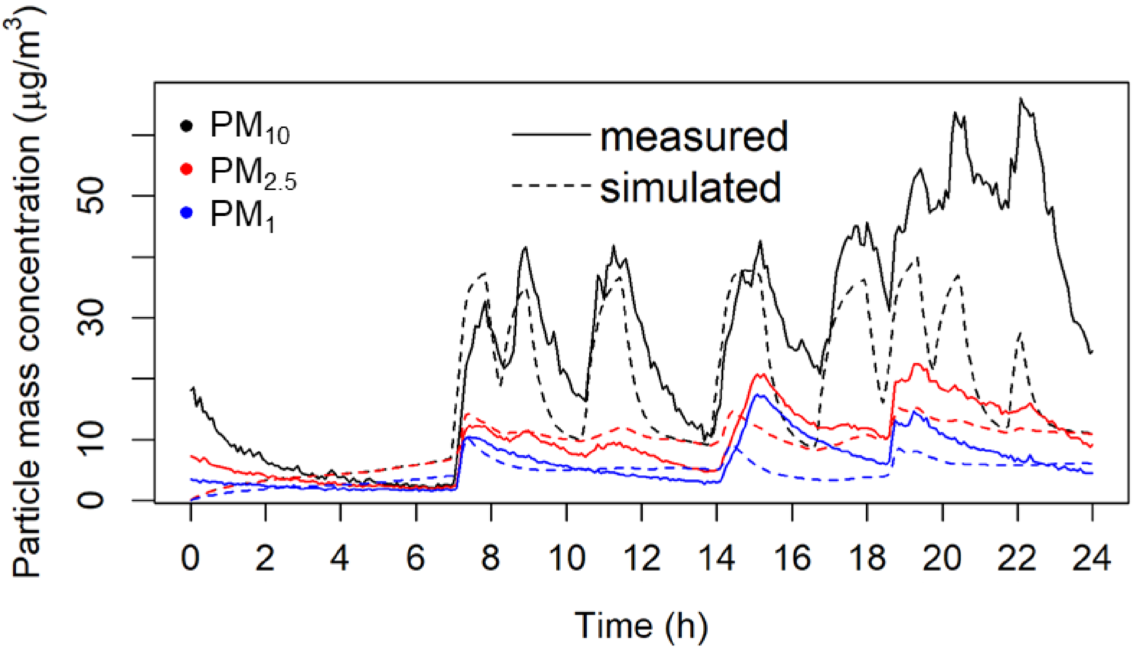

Figure S4. Comparison of measured and simulated particle mass concentration of indoor PM_1, $PM_{2.5}$ and PM_{10}.

S3 Calculation of limonene emission from wood furniture

As presented in Zhao et al.,[10] the area-specific emission rates for materials were calculated by an empirical approach with a first-order exponential model. Emission characteristics of indoor furniture and building materials were analyzed using general emission data available at Fraunhofer WKI. The area-specific emission rate (SER_A in µg m^{-2} h^{-1}) of limonene from wood furniture follows the exponential decay function $f(t) = 5 + 12 \times \exp(-t / 17.1)$, where t is time in unit of day. Considering that the furniture was not new, as shown in **Figure S5**, the SER_A is already approaching 5 µg m^{-2} h^{-1} after 20 days.

According to Fechter et al.,[11] the limonene emission from wooden furniture between 17 °C and 28 °C was estimated to increase by 135%. The change factor f for the temperature-dependent limonene emission is calculated as the coefficient of the linear regression. The temperature-dependent limonene emissions can be thus calculated by using the actual temperature and the change factor.

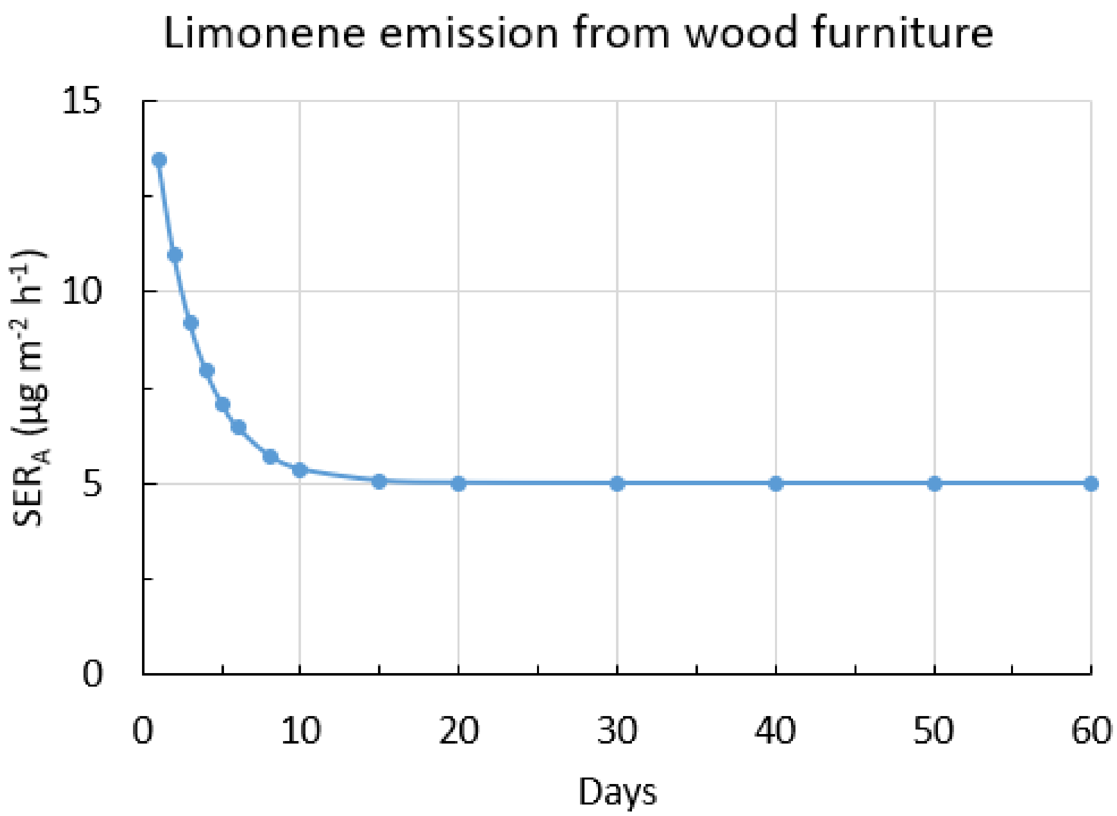

Figure S5. Limonene emission rate from wood furniture under the exponential decay function: $f(t) = 5 + 12 \times \exp(-t /17.1)$.[10]

S4 Calculation of deposition and coagulation

As mentioned in manuscript Section 2.3 “Deposition”, the particle size-resolved deposition velocity v_d was computed using the approach of Lai and Nazaroff[12] and Seinfeld and Pandis,[13] taking into account gravitational settling, Brownian diffusion and eddy diffusion, with the estimated friction velocity near indoor surfaces (u), particle diameter and temperature as inputs.

The model assumes that the particle flow is one-dimensional and steady, and assumes that Brownian diffusion and turbulent diffusion control the transport of particles through the boundary layer to the vertical surface. The surface is assumed to be a perfect settling tank, i.e., no particle resuspension is considered.[12] The relevant equations are listed as follows:

Deposition velocity for a vertical surface:

$$v_{dv} = \frac{u^*}{I}$$

Deposition velocity for an upward horizontal surface:

$$v_{du} = \frac{v_s}{1 - \exp\left(-\frac{v_s I}{u^*}\right)}$$

Deposition velocity for a downward horizontal surface:

$$v_{dd} = \frac{v_s}{\exp\left(\frac{v_s I}{u^*}\right) - 1}$$

Here:

$$I = 3.64\, S_c^{\frac{2}{3}}(a - b) + 39$$

$$a = \frac{1}{2}\ln\frac{(10.92\, S_c^{-\frac{1}{3}} + 4.3)^3}{S_c^{-1} + 0.0609} + \sqrt{3}\tan^{-1}\frac{8.6 - 10.92 S_c^{-\frac{1}{3}}}{\sqrt{3}\, 10.92\, S_c^{-\frac{1}{3}}}$$

$$b = \frac{1}{2}\ln\frac{(10.92\, S_c^{-\frac{1}{3}} + r^+)^3}{S_c^{-1} + 7.669\times 10^{-4}(r^+)^3} + \sqrt{3}\tan^{-1}\frac{2r^+ - 10.92 S_c^{-\frac{1}{3}}}{\sqrt{3}\, 10.92\, S_c^{-\frac{1}{3}}}$$

Schmidt number $S_c = \nu/D$, where ν is the kinematic viscosity of air and D is the Brownian diffusivity;

$D = kTC_c/3\pi\mu D_p$, where k is Boltzmann's constant; D_p is particle diameter; C_c is the slip correction factor = $1+2\lambda_{air}/D_p(1.257+0.4\exp(-1.1D_p/2/\lambda_{air}))$;

$\nu = \mu/\rho$, where $\mu = 1.8\times10^{-5}\,(T/298)^{0.85}$ is the dynamic viscosity of air, T is in K, and $\rho = p/R/T$ is the density of air, p is absolute pressure, R is the specific gas constant for dry air;

$r^+ = D_p u^*/2\nu$, where u^* is friction velocity;

v_s is the gravitational settling velocity of the particle.

As mentioned in manuscript Section 2.3 “Coagulation”, The coagulation coefficient K was computed based on Fuchs theory in the transition region and the free molecule region, assuming that all collisions lead to coagulation of the two colliding particles, with particle diameter and temperature as inputs.[13] For the particles with sizes D_{p1} and D_{p2}, the coagulation coefficient K_{12} can be calculated as follows:

$$K_{12} = 2\pi(D_1 + D_2)(D_{p1} + D_{p2})\left(\frac{D_{p1} + D_{p2}}{D_{p1} + D_{p2} + 2(g_1^2 + g_2^2)^{\frac{1}{2}}} + \frac{8(D_1 + D_2)}{(\bar{c}_1^2 + \bar{c}_2^2)^{\frac{1}{2}}(D_{p1} + D_{p2})}\right)^{-1}$$

Here:

$$\bar{c} = \left(\frac{8kT}{\pi m_i}\right)^{\frac{1}{2}}$$

$$g_i = \frac{1}{3D_{pi}l_i}\left[(D_{pi}+l_i)^3 - (D_{pi}^2+l_i^2)^{\frac{3}{2}}\right] - D_{pi}$$

$$l_i = \frac{8D_i}{\pi\bar{c}_i}$$

D_i is the Brownian diffusivity mentioned above for particles of size D_{pi}; m_i is the mass of the particles of size D_{pi}.

As can be seen from the equations, the fundamental parameters in the deposition and condensation model are introduced as a function of temperature rather than constant values, including dynamic viscosity (μ), air density (ρ), and air mean free path (λ_{air}). Consequently, temperature changes due to climate change are reflected in these two processes, thus affecting the overall indoor particulate concentration.

S5 Effect of the time resolution of the outdoor particle concentration on the simulated indoor particle concentration

As described in the manuscript Section 2.5.1 “IPCC scenarios”, the initial data for outdoor PM_{10} and $PM_{2.5}$ particle mass concentrations in rural area were taken from historical annual mean values measured in Germany.[14] To assess the impact of using the daily mean or annual mean values of outdoor particle concentrations as input variables on the simulation results, a case study was conducted for the year 2022. The daily mean values of PM_{10} and $PM_{2.5}$ outdoors (Figure S6) were taken from DESN025 (Leipzig-Mitte, urban traffic), whereby the daily data for $PM_{2.5}$ are only available from 2022. The annual mean concentrations of PM_{10} and $PM_{2.5}$ for this station in 2022 are 13.4 µg m^{-3} and 9.1 µg m^{-3}, respectively.

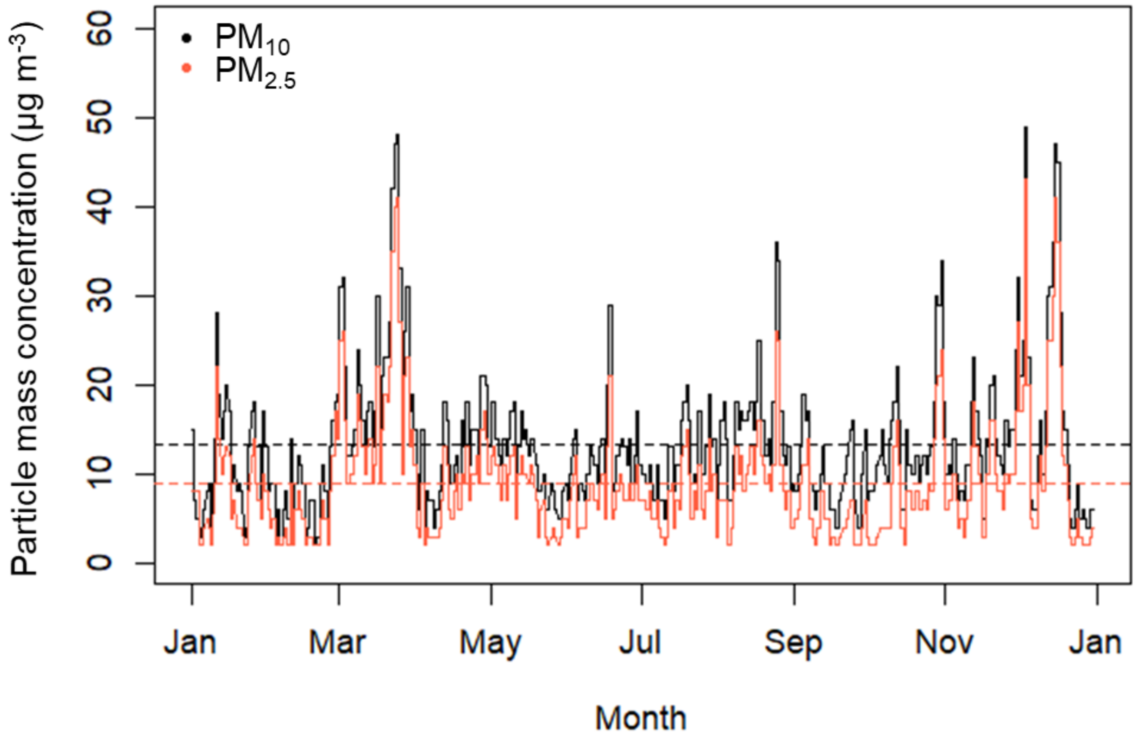

Figure S6. Outdoor PM_{10} and $PM_{2.5}$ mass concentrations (daily averages) in 2022 in Leipzig, Germany. The data for station DESN025 (Leipzig-Mitte, urban traffic) were taken from the online database of the German Environment Agency (UBA, https://www.umweltbundesamt.de/en/data). The dashed lines indicate the corresponding annual average concentrations of PM_{10} and $PM_{2.5}$.

Table **S3** lists the simulated indoor PM_{10} and $PM_{2.5}$ mass concentrations based on the two types of input data (i.e., annual and daily mean outdoor concentrations), where the annual mean indoor $PM_{2.5}$ concentrations are slightly different and PM_{10} is exactly the same. The results for the 5th, 25th and 75th percentiles also show small differences, while the results for the 95th percentile show large differences.

Since the long-term projections in this work were based on annual mean results, the effect of changes on daily outdoor particle concentrations can be neglected, especially given the uncertainty in the expected future concentrations of air pollutants.

Table S3. Simulated indoor PM_{10} and $PM_{2.5}$ mass concentrations ($\mu g\ m^{-3}$) using outdoor annual mean and daily mean values as input.

	$PM_{2.5}$ mass concentration ($\mu g\ m^{-3}$)		PM_{10} mass concentration ($\mu g\ m^{-3}$)	
	annual mean input	daily mean input	annual mean input	daily mean input
mean	6.3	6.2	8.3	8.3
5 percentiles	3.9	3.3	4.0	3.3
25 percentiles	4.4	4.2	4.4	4.3
75 percentiles	7.0	7.0	11.6	11.5
95 percentiles	11.3	13.1	17.2	18.7

S6 Particle number size distribution

S6.1 Measured and simulated outdoor particle number size distribution

The data for 2020 are based on the rural background mean values measured and published by the German Ultrafine Aerosol Network (GUAN).[15, 16] The 2100 data were calculated using the same change factors for the $PM_{2.5}$ decrease under the SSP1-2.6, SSP2-4.5, and SSP5-8.5 scenarios.

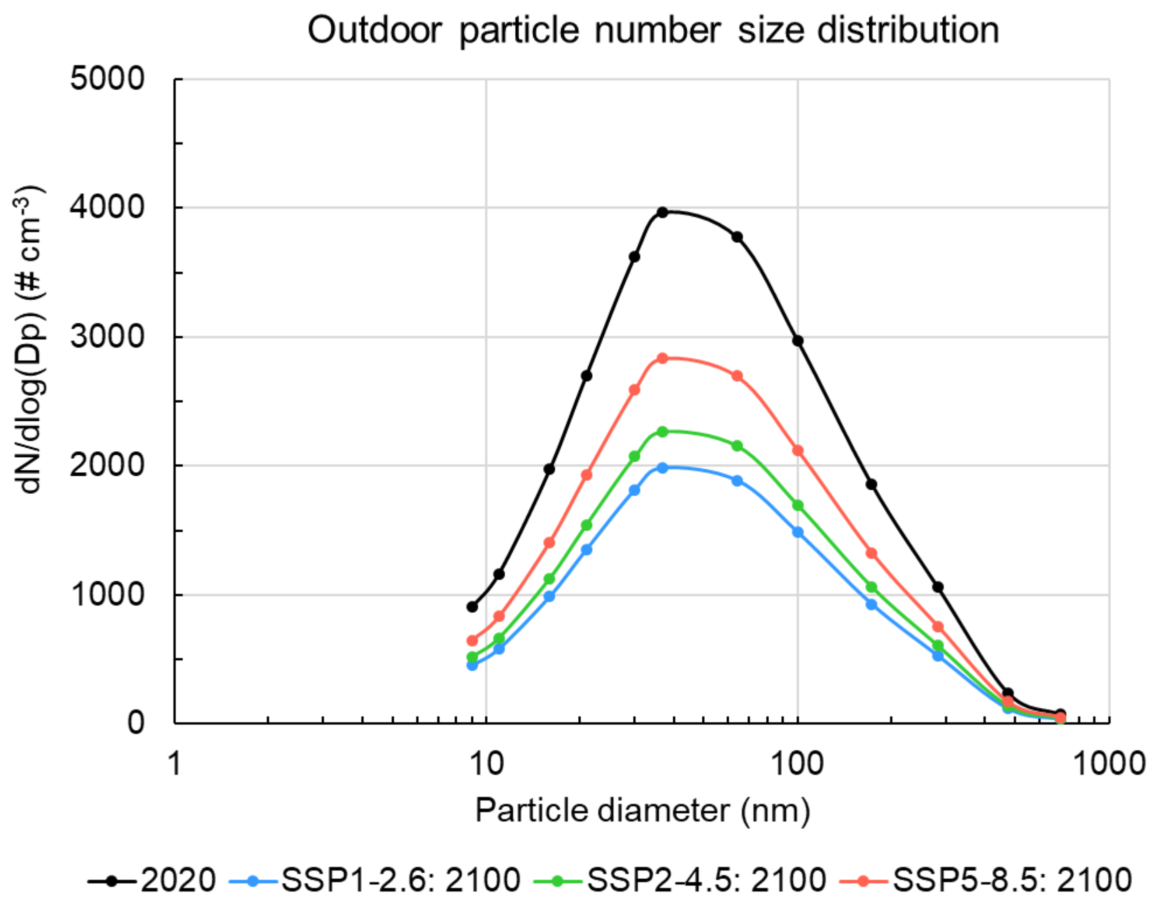

Figure S7. Outdoor PNSD in 2020 (measured) and in 2100 under different SSP climate scenarios (simulated).

S6.2 Simulated indoor particle number size distribution

Based on the outdoor PNSD in 2020 and 2100 under different SSP climate scenarios presented in S4.1, the indoor PNSD of the test house are simulated, taking into account the particle sources and losses described in Section 2.3 of the manuscript.

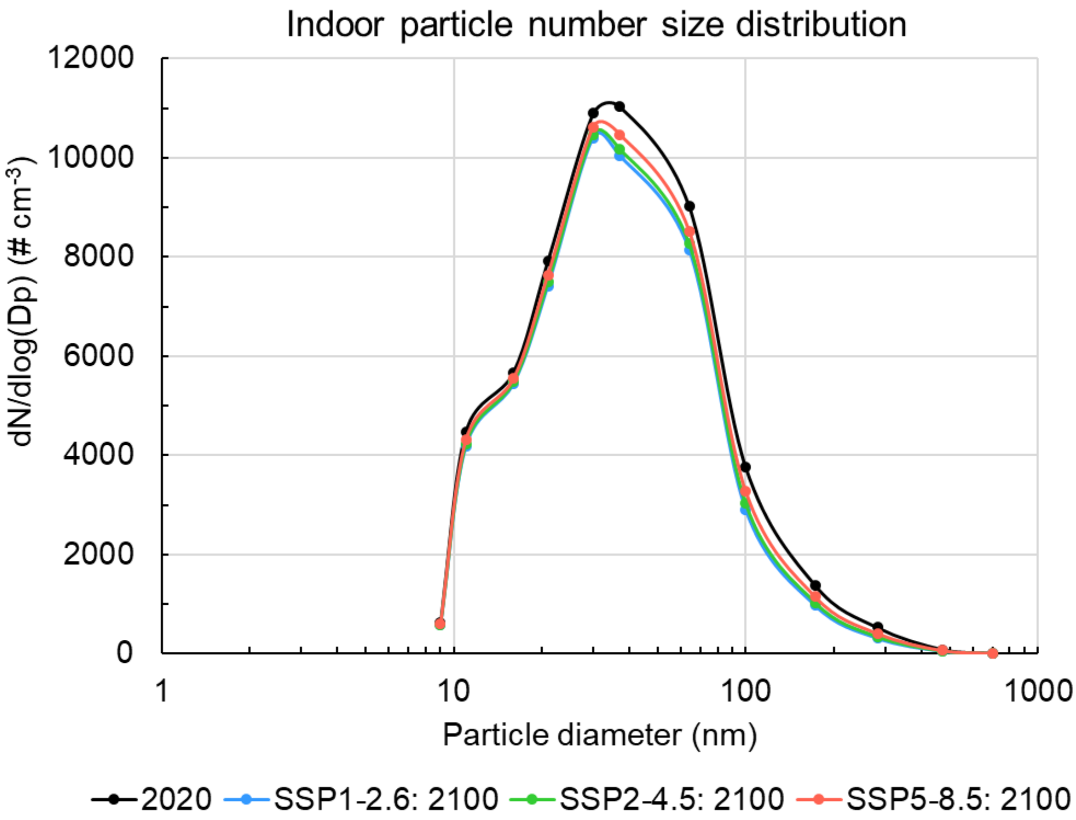

Figure S8. Simulated indoor PNSD in 2020 and in 2100 under different SSP climate scenarios.

References

1. DIN EN 779, *Particulate air filters for general ventilation - Determination of the filtration performance*, Beuth Verlag, Berlin, 2012.
2. ISO16890-1, *Air filters for general ventilation - Part 1: Technical specifications, requirements and classification system based upon particulate matter efficiency (ePM)*, International Organization for Standardization (ISO), Geneva, 2016.
3. H. Goodfellow, E. Tähti, *Industrial Ventilation Design Guidebook, 1st Edition*, Academic Press, San Diego, 2001.
4. V. Hemerka J., P. , Filter Class Conversion between EN 779 and EN ISO 16890-1, *REHVA Journa*, 2021, **01/2021**, 37-45.
5. T. Schuldt, E. Däuber, T. Engelke and F. Schmidt, Air filters for indoor environments: Interlaboratory evaluation of the new international filter testing standard ISO 16890, *Indoor Air*, 2020, **30**, 473-480, https://doi.org/10.1111/ina.12660.
6. J. Zhao, K. Weinhold, M. Merkel, S. Kecorius, A. Schmidt, S. Schlecht, T. Tuch, B. Wehner, W. Birmili and A. Wiedensohler, Concept of high quality simultaneous measurements of the indoor and outdoor aerosol to determine the exposure to fine and ultrafine particles in private homes, *Gefahrstoffe - Reinhalt. Luft*, 2018, **78**, 73-78.

7. J. Zhao, W. Birmili, B. Wehner, A. Daniels, K. Weinhold, L. Wang, M. Merkel, S. Kecorius, T. Tuch, U. Franck, T. Hussein and A. Wiedensohler, Particle Mass Concentrations and Number Size Distributions in 40 Homes in Germany: Indoor-to-Outdoor Relationships, Diurnal and Seasonal Variation, *Aerosol Air Qual. Res.*, 2020, **20**, 576-589, https://doi.org/10.4209/aaqr.2019.09.0444.

8. J. Zhao, W. Birmili, T. Hussein, B. Wehner and A. Wiedensohler, Particle number emission rates of aerosol sources in 40 German households and their contributions to ultrafine and fine particle exposure, *Indoor Air*, 2021, 31, 818-831, https://doi.org/10.1111/ina.12773.

9. T. Salthammer, J. Zhao, A. Schieweck, E. Uhde, T. Hussein, F. Antretter, H. Künzel, M. Pazold, J. Radon and W. Birmili, A holistic modeling framework for estimating the influence of climate change on indoor air quality, *Indoor Air*, 2022, **32**, e13039, https://doi.org/10.1111/ina.13039.

10. J. Zhao, E. Uhde, T. Salthammer, F. Antretter, D. Shaw, N. Carslaw and A. Schieweck, Long-term prediction of the effects of climate change on indoor climate and air quality, *Environ. Res.*, 2024, **243**, 117804, https://doi.org/10.1016/j.envres.2023.117804.

11. J.-O. Fechter, F. Englund and A. Lundin, Association between temperature, relative humidity and concentration of volatile organic compounds from wooden furniture in a model room, *Wood Mater. Sci. Eng.*, 2006, **1**, 69-75, https://doi.org/10.1080/17480270600900551.

12. A. C. K. Lai and W. W. Nazaroff, Modeling indoor particle deposition from turbulent flow onto smooth surfaces, *J. Aerosol Sci*, 2000, **31**, 463-476, https://doi.org/10.1016/S0021-8502(99)00536-4.

13. J. H. Seinfeld and S. N. Pandis, *Atmospheric Chemistry and Physics*, John Wiley & Sons, New York, 2016.

14. European Environment Agency, Air Quality e-Reporting, https://www.eea.europa.eu/data-and-maps/data/aqereporting-9, (accessed 02.03.2022).

15. W. Birmili, K. Weinhold, F. Rasch, A. Sonntag, J. Sun, M. Merkel, A. Wiedensohler, S. Bastian, A. Schladitz, G. Löschau, J. Cyrys, M. Pitz, J. Gu, T. Kusch, H. Flentje, U. Quass, H. Kaminski, T. A. J. Kuhlbusch, F. Meinhardt, A. Schwerin, O. Bath, L. Ries, H. Gerwig, K. Wirtz and M. Fiebig, Long-term observations of tropospheric particle number size distributions and equivalent black carbon mass concentrations in the German Ultrafine Aerosol Network (GUAN), *Earth Syst. Sci. Data*, 2016, **8**, 355-382, https://doi.org/10.5194/essd-8-355-2016.

16. J. Sun, W. Birmili, M. Hermann, T. Tuch, K. Weinhold, G. Spindler, A. Schladitz, S. Bastian, G. Löschau, J. Cyrys, J. Gu, H. Flentje, B. Briel, C. Asbach, H. Kaminski, L. Ries, R. Sohmer, H. Gerwig, K. Wirtz, F. Meinhardt, A. Schwerin, O. Bath, N. Ma and A. Wiedensohler, Variability of black carbon mass concentrations, sub-micrometer particle number concentrations and size distributions: results of the German Ultrafine Aerosol Network ranging from city street to High Alpine locations, *Atmos. Environ.*, 2019, **202**, 256-268, https://doi.org/10.1016/j.atmosenv.2018.12.029.